

EXTENDED ROTATION CURVES OF HIGH-LUMINOSITY SPIRAL GALAXIES. II. THE ANEMIC Sa GALAXY NGC 4378

VERA C. RUBIN* AND W. KENT FORD, JR.

Department of Terrestrial Magnetism, Carnegie Institution of Washington

K. M. STROM AND S. E. STROM

Kitt Peak National Observatory†

AND

W. ROMANISHIN

Steward Observatory, University of Arizona; and Kitt Peak National Observatory†

Received 1978 January 18; accepted 1978 March 22

ABSTRACT

Spectroscopic and photometric observations are reported for the Sa galaxy NGC 4378. Our data suggest that this galaxy is located at a distance of ~ 50 Mpc; if so, its absolute blue luminosity $M_B = -21.1$. From an analysis of its rotation curve, a total mass, $\mathfrak{M} = 3.6 \pm 0.5 \times 10^{11} \mathfrak{M}_\odot$, is derived. The mass to blue-luminosity ratio increases from $\mathfrak{M}/L_B = 4.0$ for regions within 2 kpc of the nucleus to $\mathfrak{M}/L_B \approx 10$ in the outer regions of the galaxy. The hydrogen-mass to blue-luminosity ratio, $\mathfrak{M}_{\text{H I}}/L_B \approx 0.1$, is quite typical of early-type galaxies.

Star formation in NGC 4378 follows a pattern qualitatively similar to that in our own Galaxy. Newly formed stars are virtually absent in the nuclear bulge region but increase in relative number out to a radius of ~ 18 kpc, beyond which the star-formation rate drops. Ionized hydrogen regions in NGC 4378 show a ratio $[\text{N II}]/\text{H}\alpha$ which drops below unity only beyond 10 kpc. This result suggests that metal enrichment in the disk of this galaxy may have proceeded to a greater degree and over a larger fraction of the disk than is typical of other early-type galaxies. NGC 4378 has been called an "anemic" spiral by van den Bergh. This classification appears to result from the combined influences of a somewhat fainter than normal disk surface brightness and a lower star-forming efficiency in its arms.

Subject headings: galaxies: individual — galaxies: internal motions — galaxies: photometry — galaxies: stellar content — galaxies: structure

I. INTRODUCTION

NGC 4378 is one of the finest examples of a relatively nearby Sa galaxy. A prominent nuclear bulge region is surrounded by a disk which contains a single, tightly wound, faint spiral arm composed of many knotlike emission regions. In Figure 1 (Plate 7) we reproduce a Mayall 4 m prime-focus photograph of this galaxy. Visual comparison of this galaxy with other, better-known early-type spiral galaxies, such as M31 and M81, suggests that the arm amplitude and average disk surface brightness are unusually low in NGC 4378. Consequently, NGC 4378 is classified as an early-type, anemic spiral (Ab II:) in van den Bergh's (1976) modification of the Hubble system; this classification is meant to suggest that the current star-forming activity in the spiral-arm regions is ab-

normally low. Although van den Bergh evidently prefers placing NGC 4378 in the Hubble "b-type" category, we believe its morphological appearance to be more consistent with the more conventional "a-type" classification (Sandage 1961; Nilson 1973; de Vaucouleurs, de Vaucouleurs, and Corwin 1976).

Because of both its early type and its anemic appearance, we felt that a detailed study of this system was merited. At present, the total mass and mass distribution are known for only a few spiral systems of very early Hubble type. Furthermore, there exists very little information regarding either the distribution of newly formed stars or the properties of H II regions in a-type galaxies.

Finally, there is as yet no physical understanding of the "anemic" phenomenon in spiral galaxies; indeed, we are not able to judge by visual inspection the degree to which this characteristic results from a lower than normal disk surface brightness, a low rate of star formation in the arms, or possibly both.

In the following sections we report the results of a spectroscopic and photometric study designed to determine many of the basic physical characteristics of this galaxy.

* Visiting Astronomer, Cerro Tololo Inter-American Observatory, operated by the Association of Universities for Research in Astronomy, Inc., under contract with the National Science Foundation.

† Operated by the Association of Universities for Research in Astronomy, Inc., under contract with the National Science Foundation.

TABLE 1a
4 m SPECTROSCOPIC OBSERVATIONS OF NGC 4378

Spect. Plate*	Date	Exp. (min)	PA (°)	Lines Measured; Extent
C455	1977 Mar 24	148	148	H α , [N II] λ 6583; 18" NW to 58" SE
C460a	1977 Mar 25	20	7.5	[N II] λ 6583; 2"3 NE to 1"8 SW
C460b	1977 Mar 25	10	7.5	[N II] λ 6583; nucleus
C460c	1977 Mar 25	5	7.5	[N II] λ 6548, 6583; nucleus
C466	1977 Mar 26	150	180	H α , [N II] λ 6583; 90" N to 67" S

*IIIa-J, N₂ baked + preflashed; image-tube transfer optics $f/2$; slit width 200 μ = 1"3; dispersion = 50 \AA mm⁻¹.

II. VELOCITY AND MASS DISTRIBUTION IN NGC 4378

Intensity-calibrated spectra of the nucleus and outer disk of NGC 4378 were obtained with the CTIO 4 m Ritchey-Chrétien spectrograph plus Carnegie image tube. A record of the observations is given in Table 1, and two of the spectra are reproduced in Figure 1. From an average of three spectra of the nucleus, a systemic heliocentric velocity $V = 2540 \pm 12 \text{ km s}^{-1}$ is measured; this corresponds to $V_0 = 2427 \text{ km s}^{-1}$ reduced to the Local Group (with $\Delta V = 300 \sin l \cos b \text{ km s}^{-1}$; see de Vaucouleurs *et al.*). This value is in excellent agreement with $V_0 = 2423 \text{ km s}^{-1}$ derived by Krumm and Salpeter (1976) from 21 cm observations (but in apparently less satisfactory agreement with the optical velocity $V = 2359 \text{ km s}^{-1}$ which they quote [Sandage 1977]). Although NGC 4378 is apparently located on the outskirts of the Virgo cluster, its observed velocity would make it one of the highest-velocity members. Rather than place it at the mean distance of the cluster ($r \approx 20$ Mpc), we adopt a distance of 49 Mpc, based on $V_0 = 2427 \pm 10 \text{ km s}^{-1}$ and $H = 50 \text{ km s}^{-1} \text{ Mpc}^{-1}$. At this distance, $1'' = 238 \text{ pc}$.

The position angle of the major axis of NGC 4378 is measured as $164^\circ \pm 3^\circ$. The inclination i to the line of sight has been determined visually by measuring the axial ratio of the ellipse formed by the outer arm on the plane of the sky, assuming that the galaxy is a circle in its principal plane; we obtain $i = 35^\circ \pm 3^\circ$. The ellipticity of the isophotes in U and R , discussed below and shown in Table 2, is also used to establish the inclination of the galaxy (and we derive $i_U = 33^\circ \pm 1^\circ$, $i_R = 35^\circ \pm 1^\circ$). The value $i = 35^\circ$ which we adopt does not agree with the minor-

major-axis ratio given by Nilson (1973) and de Vaucouleurs *et al.*, which implies $i = 19^\circ$, i.e. close to face-on. Such a low inclination is inconsistent with the measured ellipticity and produces rotational velocities which are unacceptably high.

We chose to obtain spectra at P.A. = 148° and P.A. = 180° in order that the slit might pass through suspected emission knots. Because each of these position angles is located 16° from the major axis, velocities from both position angles can be combined into a mean rotation curve. Velocities on the plane of the sky measured from H α and from [N II] are listed in Table 3 and plotted in Figure 2. H α is redshifted to a region free of night-sky emission, but [N II], at a velocity of 2320 km s^{-1} , will blend with the night-sky $\lambda 6634.31$ line (Peterson *et al.* 1976). Consequently, no velocities lower than $V = 2355 \text{ km s}^{-1}$ have been measured from this line. Although all galaxian emission is rather weak, we estimate that the measured velocities should be accurate to better than 15 km s^{-1} at most points.

Rotational velocities $V(r)$ in the plane of the galaxy, calculated from the expression

$$V(r) = (V_{\text{obs}} - 2540) \times \frac{(\sec^2 i - \tan^2 i \cos^2 16^\circ)^{1/2}}{\sin i \cos 16^\circ},$$

are also listed in Table 2 and plotted in Figure 3. The velocities rise steeply across the nucleus to a peak velocity of 320 km s^{-1} at $r \leq 3 \text{ kpc}$ and then decrease slowly as $V \sim r^{-0.05}$ to $V = 286 \text{ km s}^{-1}$ at $r = 22 \text{ kpc}$. A velocity maximum as high as $V_{\text{max}} = 320 \text{ km s}^{-1}$ is known for only one other galaxy, NGC 4595, the Sombrero (Schweizer 1978), also an Sa.

TABLE 1b
4 m PRIME-FOCUS OBSERVATIONS OF NGC 4378

Prime Focus Plate	Date	Exp. (min)	Filter	Emulsion*	Development
MPF 2384	1977 May 18	50	RG 610 (R)	127-04	D-19 5 min
MPF 2385	1977 May 18	100	UG 2 (U)	IIIa-J	D-19 5 min

*N₂ baked, hydrogen treated.

TABLE 2
OBSERVED ELLIPTICITY AND CALCULATED
INCLINATION IN U AND R AS A FUNCTION OF
MINOR-AXIS DISTANCE FOR NGC 4378

	b (arcsec)	b/a	$t = \cos^{-1} b/a$
U	7.270	0.846	32.2
	12.252	0.802	36.7
	18.090	0.817	35.2
	25.568	0.774	39.3
	36.602	0.792	37.6
	81.515	0.841	32.8
R	4.395	0.874	29.1
	7.908	0.855	31.2
	12.340	0.809	36.0
	18.737	0.823	34.6
	29.424	0.819	35.0

Note that the outermost emission knot ($r = 22$ kpc) for which a velocity was measured coincides closely with the outer edge of the most distant arm visible in Figure 1.

The mass distribution in NGC 4378 can be determined from the observed rotation curve and a suitable model. We initially make the usual assumption that the gas is restricted to a flattened disk, so that the rotational velocities are equivalent to circular velocities. An assessment of the validity of this assumption is made below. We calculated the mass distribution within NGC 4378 for three idealized models: (1) a pure disk, (2) a pure spheroid with axial ratio $c/a = 0.4$, and (3) a composite model characterized by a spheroidal bulge ($c/a = 0.8$) and a disk ($c/a = 0.2$). For models (2) and (3), we adopted the density distribution given by a simple model, $\rho = \rho_0/[1 + (r/r_0)^n]$, where the central density ρ_0 , scale length r_0 , and exponent n are adjusted to reproduce the observed velocities. Because the derived mass properties of the single spheroid model turn out to be intermediate between models (1) and (3), we discuss below only these two models. The solid line in Figure 3 is a curve drawn through mean velocities for small ranges of r ($r < 6$ kpc) and is an eye estimate for $r > 10$ kpc.

With the assumption of disk geometry (model [1]) and this rotation curve, the Kuzmin (1952) integral

TABLE 3
MEASURED HELIOCENTRIC VELOCITIES IN NGC 4378

Plate Line	Plane of Sky		Plane of Galaxy		Plate Line	Plane of Sky		Plane of Galaxy	
	Y (arcsec)	V (km s ⁻¹)	r^* (kpc)	$V(r)^\dagger$ (km s ⁻¹)		Y (arcsec)	V (km s ⁻¹)	r^* (kpc)	$V(r)^\dagger$ (km s ⁻¹)
<u>C460a</u>					<u>C466</u>				
[N II]	NE - 2.3	2667	0.56	235	H α	N -90.5	2687	21.88	272
	0	2519	0	21		-85.9	2696	20.76	289
	SW + 1.8	2441	0.44	183		-79.3	2697	19.17	290
						-75.8	2703	18.34	302
						-64.9	2706	15.70	307
<u>C460b</u>						-47.9	2742	11.59	374
[N II]	0	2560	0	11		-44.3	2708	10.71	311
						- 6.7	2729	1.62	350
<u>C460c</u>						+ 4.7	2366	1.14	322
[N II]	0	2541	0	1		+ 7.1	2388	1.71	281
						+64.3	2397	15.56	265
					S	+66.5	2379	16.08	298
<u>C455</u>					[N II]	N -85.5	2700	20.67	296
H α	NW - 4.6	2687	1.12	272		-24.6	2707	5.94	309
	+ 4.6	2395	1.12	268		-19.8	2709	4.80	313
	+ 6.4	2389	1.54	279		-15.2	2715	3.68	324
	+43.5	2372	10.52	311		- 5.3	2731	1.28	353
	+46.6	2384	11.26	289		+ 5.2	2398	1.26	263
	SE +58.1	2403	14.04	253		+11.0	2369	2.66	316
					S	+22.6	2371	5.46	313
[N II]	NW -17.6	2700	4.25	296					
	-12.9	2708	3.11	311					
	- 8.1	2716	1.95	326					
	- 4.4	2692	1.07	281					
	+ 4.8	2379	1.16	298					
	+ 8.2	2373	1.97	309					
	+12.9	2357	3.11	339					
	+17.5	2355	4.23	342					
	SE +22.6	2360	5.46	333					

$$*r = Y(\sec^2 t - \tan^2 t \cos^2 16^\circ)^{1/2}$$

$$^\dagger V(r) = (V_{\text{obs}} - 2540)(\sec^2 t - \tan^2 t \cos^2 16^\circ)^{1/2} / \sin t \cos 16^\circ$$

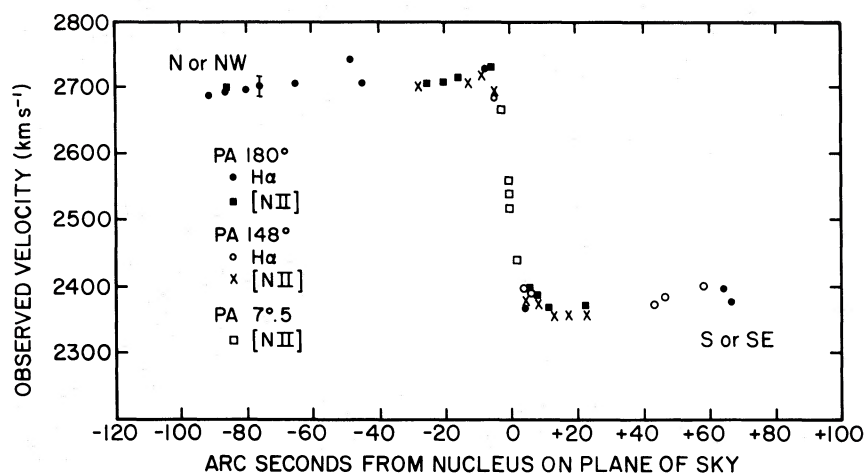


FIG. 2.—Observed velocities in NGC 4378 as a function of nuclear distance

can be solved and gives a mass $\mathfrak{M} = 2.8 \times 10^{11} \mathfrak{M}_{\odot}$ to $r = 22$ kpc. Brandt (1960) has shown that masses based on pure disk models are always underestimates; he suggests an increase by the factor 1.1. Adopting this correction factor, we derive $\mathfrak{M} = 3.0 \times 10^{11} \mathfrak{M}_{\odot}$. The adopted velocities and the resulting mass as a function of r are shown in columns (2) and (3) of Table 4.

While a disk model for NGC 4378 is acceptable for the outer regions, it is a poor approximation near the bulge. Evidence that the scale height of the gas is relatively large in the bulge region comes primarily from the large observed velocity dispersion. The emission lines in the nucleus ($r < 475$ pc) of NGC 4378 show a velocity dispersion (corrected for instrumental

broadening and the line-of-sight circular-motion component) of $\sigma_V = 190 \pm 25 \text{ km s}^{-1}$. This value of σ_V is comparable to the stellar velocity dispersion in the nuclear bulge region inferred from measurement of the Na D absorption line width. Random motions in the gas as large as those in the stellar population are surprising and suggest that the gas is not restricted to a flattened disk. Order-of-magnitude calculations (based on the model discussed by Burbidge, Burbidge, and Prendergast 1959) indicate that the mean density near the nucleus comes from two equal terms: one due to the rotation and one due to the "pressure" equivalent of the random motions. This implies that, for galactocentric distance $r \lesssim 1$ kpc, the mass should be doubled to account for the amount by

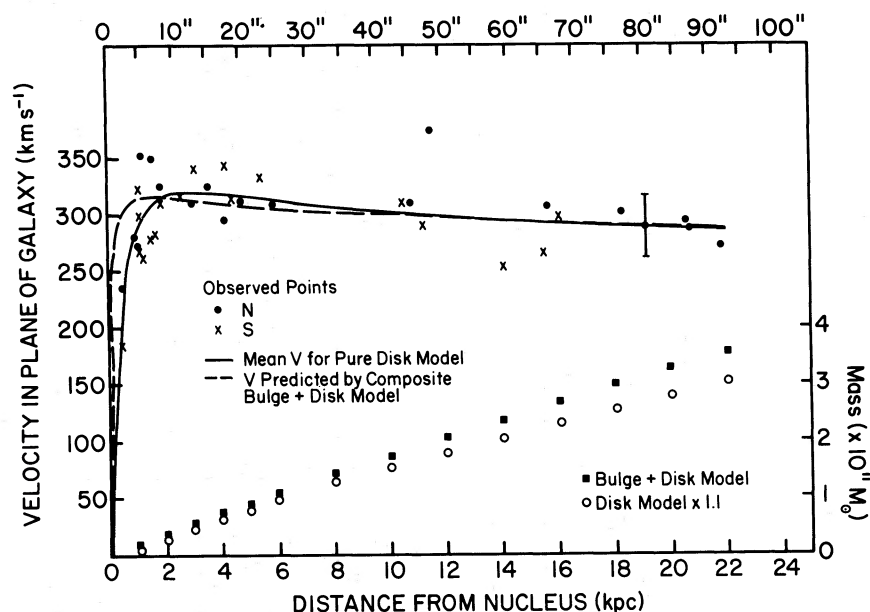


FIG. 3.—Rotational velocities in NGC 4378 as a function of nuclear distance. *Solid line*, adopted velocities for disk model; *broken line*, predicted velocities for bulge-plus-disk model. *Lower*, integrated mass as a function of distance from the nucleus for disk model and for composite model.

TABLE 4
 MASS MODELS FOR NGC 4378

Disk Model			Bulge ($c/a = 0.8$) Plus Disk ($c/a = 0.2$) Model						
R (kpc) (1)	V (km s ⁻¹) (2)	$\int M(r) \times 1.1$ (10 ¹¹ M_{\odot}) (3)	V (km s ⁻¹) (4)	$\int M(r)$ (10 ¹¹ M_{\odot}) (5)	V_I^* (km s ⁻¹) (6)	V_{II} (km s ⁻¹) (7)	$\int M_I(r)^\dagger$ (10 ¹¹ M_{\odot}) (8)	$\int M_{II}(r)$ (10 ¹¹ M_{\odot}) (9)	Face-on Surface Density [‡] (10 ⁸ M_{\odot} kpc ⁻²) (10)
0	0	0	0	0	0	0	0	0	
0.1			210	0.009	196	76	0.008	0.0007	222:
0.4	180	0.013	292	0.064±0.05	234	175	0.042	0.018	64±31
1	278	0.096	313	0.19±0.09	235	206	0.12	0.067	25±36
2	316	0.30	314	0.38±0.08	231	213	0.23	0.15	12±9
3	320	0.48	312	0.56±0.08	228	213	0.33	0.22	7.4±4.1
4	318	0.64	309	0.74±0.10	225	213	0.44	0.30	5.4±2.3
5	316	0.81	307	0.91±0.10	223	212	0.54	0.37	4.2±1.5
6	313	0.96	305	1.09±0.13	221	211	0.64	0.45	3.5±1.0
8	307	1.26	302	1.42±0.16	218	209	0.83	0.59	2.5±0.5
10	302	1.53	299	1.74±0.21	216	207	1.02	0.72	2.0±0.3
12	298	1.80	297	2.06±0.26	214	206	1.20	0.86	1.6±0.2
14	294	2.05	295	2.37±0.32	213	205	1.38	0.99	1.4±0.1
16	292	2.31	293	2.68±0.37	211	203	1.56	1.12	1.2±0.1
18	290	2.56	292	2.99±0.43	210	202	1.73	1.25	1.0±0.1
20	288	2.80	290	3.29±0.49	209	202	1.91	1.38	0.93±0.07
22	286	3.05	289	3.58±0.53	208	201	2.08	1.50	0.83±0.06

*Contribution to V from each component, $V = (V_I^2 + V_{II}^2)^{1/2}$.

†Contribution to $\int M(r)$ from each component.

‡Divide by 17.72 for surface density in M_{\odot} arcsec⁻².

which the rotational velocities are lower than the circular velocities. Hence the total corrected mass for a pure disk model becomes $3.1 \times 10^{11} M_{\odot}$.

The above discussion, combined with the optical appearance of the galaxy, suggests that the composite "bulge-disk" model might be more realistic. In Figure 3 the broken line indicates the velocities that are predicted by a mass model which is the sum of two components, the first a spheroidal bulge and the second a flattened disk, with densities given by:

$$\rho_I(r) = \frac{10^{12}}{1 + (r/0.04)^{2.1}} M_{\odot} \text{ kpc}^{-3}, \quad c/a = 0.8,$$

$$\rho_{II}(r) = \frac{10^{11}}{1 + (r/0.2)^{2.1}} M_{\odot} \text{ kpc}^{-3}, \quad c/a = 0.2. \quad (1)$$

Note that the scale length for the disk component is 5 times that for the bulge component. The results for this model are contained in columns (4)–(10) of Table 4. Consecutive columns list the calculated velocity, the integrated mass, the contribution to the velocity from each of the mass components, the contribution to the integrated mass from each component, and the surface density at each r when the galaxy is viewed face-on ($i = 90^\circ$). The total mass, which increases almost linearly with r to $M = 3.6 \pm 0.5 \times 10^{11} M_{\odot}$, comes 60% from the bulge and 40% from the disk. While this model is in no sense unique, it is a simple, physically plausible one, which reproduces the observed velocities very well for $r > 2$ kpc. Interior to $r = 2$ kpc, the predicted velocities are all higher than

the observed velocities; this discrepancy is in the right direction to account for the neglected pressure term; hence no additional correction is included. The integrated mass for both the disk and the composite models is plotted in Figure 3. We will use the mass distribution derived for the composite model to study the mass-to-light variation across NGC 4378 in § IV. The error in the mass estimate is chosen equal to the mass difference between the composite and the disk models.

We note that the ratio of halo mass to disk mass, $M_H/M_D \approx 1.5$, derived from the composite model is consistent with the value required by Ostriker and Peebles (1973) to stabilize the disk against bar instabilities. A similar value, $M_H/M_D \gtrsim 1.5$, was derived from analysis of the disk and halo light distribution of the S0 galaxy NGC 3115 by Strom *et al.* (1977).

III. SURFACE BRIGHTNESS PROFILES, COLORS, AND EMISSION-LINE STRENGTHS

To study variations in the population mix and mass-to-light ratio in NGC 4378, we obtained a set of photoelectric and photographic observations of this galaxy.

In Table 5 we present the U , B , V , and R magnitudes derived for this galaxy from observations made at the KPNO 1.3 m telescope through circular aperture diameters 16"4 and 30"4 and centered on the nucleus. Corrections for extinction within our own Galaxy were made according to the prescription $A \csc |b|$, where $b = 66^\circ 9$ is the galactic latitude of NGC 4378 and $A = 0.16, 0.13, 0.10$, and 0.07 for U , B , V , and R , respectively.

TABLE 5
NUCLEAR PHOTOELECTRIC U , B , V , AND R MEASUREMENTS FOR NGC 4378 COMPARED
WITH NGC 3115, NGC 4594, AND M31

Dia. Size	NGC 4378		NGC 3115*	NGC 4594*	M31†
	30"4	16"4	21"	106"	7"62
U	14.16±0.03	14.73±0.04			
B	13.56±0.02	14.08±0.02			
V	12.59±0.02	13.10±0.02			
R	11.79±0.02	12.27±0.02			
$(U - B)_0$	0.57±0.04	0.62±0.05	0.58	0.525	0.66
$(B - V)_0$	0.94±0.02	0.95±0.02	0.95	0.95	0.92
$(V - R)_0$	0.77±0.02	0.80±0.02			0.80
$(U - R)_0$	2.28±0.02	2.37±0.02			

*de Vaucouleurs (1961).

†Sandage, Becklin, and Neugebauer (1969) with $A_V = 0.4$ (van den Bergh 1968).

The resulting colors $(U - B)_0$, $(B - V)_0$, and $(V - R)_0$ are also listed in Table 5. Note that the observed values of $(U - B)_0$ and $(B - V)_0$ for NGC 4378 are quite similar to the values observed for typical E and S0 nuclei (de Vaucouleurs 1961).

The radial dependence of U and R surface brightness was derived from analysis of photographs taken in these bandpasses at the prime focus of the Mayall 4 m reflector; the plate-filter combinations and exposure times are summarized in Table 1. By using the SURFBRT routines developed by Strom and Strom (1977) for the KPNO interactive picture processing system (IPPS), we obtained at each galactocentric distance r (measured along the major axis) the surface brightness averaged over an elliptical isophote of axial ratio $c/a = 0.80$. In Table 6 we list our derived U and R surface brightness values. The listed errors represent standard deviations in the derived mean intensity value for a given isophote and include implicitly the effects of plate and quantum noise. The transformation to the U and R system was effected by comparison of simulated aperture photometry (Strom and Strom 1977) of our photographic data with the observed values listed in Table 5. We estimate that the precision of tabulated surface brightness values exceeds ± 0.1 mag for $R < 25$ mag arcsec $^{-2}$, while the $U - R$ colors should be accurate to better than ± 0.2 mag for this range in surface brightness.

In Figure 4 we plot the U and R profiles as a function of r ; note that the U profile has been normalized to match the R profile at $r = 55''$. This figure illustrates well both the location and the blueness of the spiral-arm features at $r = 62''$ and $r = 87''$. The contribution of the nuclear bulge to the observed surface brightness distribution can be estimated by plotting the U and R distributions against $r^{1/4}$. De Vaucouleurs (1959) and Kormendy (1977) have shown that an $r^{1/4}$ falloff adequately describes the light distribution both for E galaxies and for the nuclear bulges of S0's. Over the nuclear bulge, interior to $r \approx 30''$ (7 kpc),

the $r^{1/4}$ law provides an excellent match to our data; thereafter, out to the edge of the galactic disk arm, $r = 92''$ (22 kpc), the surface brightness declines much more slowly. Over most of the galactic disk, $35'' < r < 90''$ (9–21 kpc), the surface brightness decreases by only 1 mag in U , less than one-half of that predicted by the $r^{1/4}$ relation. Although the disk of the galaxy is apparently faint, ~ 24.5 mag arcsec $^{-2}$ in U , it contributes quite noticeably to the derived brightness distribution for $r > 35''$. However, the light distribution does not appear to be exponential over any significant range in r ; although not typical of most spiral galaxies, nonexponential disk-light distributions have also been noted by Kormendy (1977).

Some gross characteristics of the stellar population in NGC 4378 can be inferred from the observed variations of the $U - R$ index across the galaxy.

In Figure 5a we plot $(U - R)_0$ against galactocentric distance and list the values in Table 7, column (9). Within the nuclear bulge, $(U - R)_0$ is constant at $(U - R)_0 = 2.4$ mag. With increasing nuclear distance, the blue arms become more prominent to the limit of the apparent optical image (see Fig. 1), where $(U - R)_0 = 1.6$ mag. Beyond the optical image, with the absence of the blue arms, the colors redden sharply. An equivalent description of this color variation is given by the ratio of U to R luminosity locally, L_U/L_R , in Table 7, column (8). L_U/L_R increases from 35% in the bulge to 70% at the edge of the optical image and then decreases. If we assume that $U - R$ is a measure of the relative contribution of newly formed stars, we immediately note a striking similarity between the star-forming pattern in NGC 4378 and the inner parts of our own Galaxy. Surrounding the nucleus, there is a region of low hydrogen abundance and little (or no) star formation. With increasing r , star formation and total hydrogen (H I plus H II) density increases, reaching a maximum near $r = 6$ kpc. In our Galaxy the relative contribution of newly formed stars to the disk light appears to decrease beyond this radius. The radial dependence of emission-

TABLE 6
PHOTOGRAPHIC DETERMINATION OF U AND R SURFACE BRIGHTNESS FOR NGC 4378,
UNCORRECTED FOR EXTINCTION

a (arcsec)	a (kpc)	U (mag arcsec $^{-2}$)	a (arcsec)	a (kpc)	R (mag arcsec $^{-2}$)
4.73	1.12	20.51±0.01	4.80	1.14	18.08±0.01
9.55	2.27	21.56±0.01	9.64	2.29	19.10±0.01
14.69	3.49	22.28±0.01	14.77	3.51	19.75±0.01
19.54	4.64	22.82±0.01	19.61	4.66	20.31±0.01
24.39	5.79	23.26±0.01	24.60	5.84	20.78±0.01
29.41	6.99	23.61±0.02	29.95	7.11	21.19±0.01
34.50	8.20	23.82±0.02	35.05	8.33	21.51±0.01
39.50	9.58	24.03±0.04	39.90	9.48	21.78±0.01
44.44	10.6	24.25±0.03	44.70	10.6	22.08±0.01
49.37	11.7	24.46±0.02	49.61	11.8	22.39±0.01
54.31	12.9	24.66±0.02	54.55	13.0	22.65±0.01
59.25	14.1	24.67±0.02	59.48	14.1	22.76±0.01
64.19	15.2	24.73±0.03	64.41	15.3	22.89±0.02
69.12	16.4	24.89±0.05	69.33	16.5	23.07±0.02
74.06	17.6	24.93±0.06	74.24	17.6	23.13±0.03
78.99	18.8	24.95±0.07	79.16	18.8	23.18±0.03
83.95	19.9	24.90±0.06	84.07	20.0	23.19±0.03
88.87	21.1	24.94±0.05	88.97	21.1	23.24±0.03
93.81	22.3	25.23±0.07	93.87	22.3	23.46±0.03
98.74	23.4	25.64±0.08	98.65	23.4	23.73±0.04
103.68	24.6	26.06±0.10	103.68	24.6	24.07±0.04
108.62	25.8	26.47±0.14	108.62	25.8	24.34±0.04
113.56	27.0	26.75±0.20	113.56	27.0	24.62±0.05
118.49	28.1	27.13±0.29	118.49	28.1	24.97±0.04
			123.43	29.3	25.28±0.05
			128.38	30.5	25.74±0.10
			133.31	31.7	25.99±0.19

TABLE 7

LUMINOSITIES, LOCAL MASS-TO-LUMINOSITY RATIOS, AND INTEGRAL MASS-TO-LUMINOSITY RATIOS IN NGC 4378

r (kpc) (1)	L_U^b arcsec $^{-2}$ $10^5 L_\odot$ (2)	L_R^b arcsec $^{-2}$ $10^5 L_\odot$ (3)	Local (M/L_U) (4)	Local (M/L_R) (5)	$\int L_U^b$ $10^{10} L_\odot$ (6)	$\int M / \int L_U^b$ (7)	L_U^b / L_R^b (8)	$(U - R)_0$ (9)
1.1					0.35±0.02	5.9±1.3		
2	98.6±1.3	277±11	6.9±4.0	2.4±1.5	0.55±0.02	6.8±0.8	0.35±0.01	2.39±0.01
3	57.4±0.70	165±7.1	7.3±3.1	2.6±1.1	0.74±0.02	7.4±0.6	0.34±0.01	2.41±0.01
4	34.9±0.43	104±4.6	8.7±2.9	2.9±1.0	0.93±0.04	8.0±0.6	0.34±0.01	2.43±0.01
5	24.0±0.29	70.1±3.0	9.9±2.7	3.4±0.9	1.09±0.04	8.4±0.5	0.34±0.01	2.44±0.01
6	16.9±0.25	49.4±2.0	11.7±2.6	4.0±0.9	1.18±0.04	9.1±0.6	0.34±0.01	2.42±0.01
8	11.1±0.28	28.2±1.2	12.7±2.0	5.1±0.8	1.39±0.06	10.3±0.6	0.40±0.01	2.25±0.02
10	7.9±0.34	17.9±0.76	14.2±1.7	6.2±0.7	1.58±0.06	11.0±0.7	0.43±0.01	2.17±0.03
12	5.76±0.13	11.3±0.47	15.7±1.5	7.9±0.8	1.74±0.08	11.8±0.8	0.50±0.01	2.01±0.02
14	4.97±0.12	8.5±0.35	15.9±0.9	9.4±0.6	1.90±0.10	12.5±0.9	0.59±0.01	1.83±0.02
16	4.31±0.21	6.80±0.56	15.7±1.1	10.0±0.8	2.03±0.10	13.3±1.0	0.64±0.02	1.74±0.04
18	3.82±0.29	5.79±0.73	14.8±1.3	9.7±1.0	2.19±0.10	13.7±1.0	0.65±0.04	1.73±0.07
20	4.01±0.29	5.64±0.70	13.1±0.9	9.4±0.9	2.35±0.14	14.1±1.1	0.71±0.05	1.62±0.07
22	3.21±0.25	4.65±0.57	14.6±1.1	10.1±0.9	2.50±0.16	14.2±1.1	0.69±0.05	1.65±0.08
24	1.63±0.18	2.92±0.49			2.62±0.18		0.57±0.06	1.85±0.11
26	0.89±0.16	1.85±0.32			2.69±0.20		0.46±0.07	2.09±0.17
28	0.50±0.18	1.15±0.20			2.73±0.22		0.46±0.12	2.10±0.29

Note: Quantities in columns (2)-(5) are face-on values.

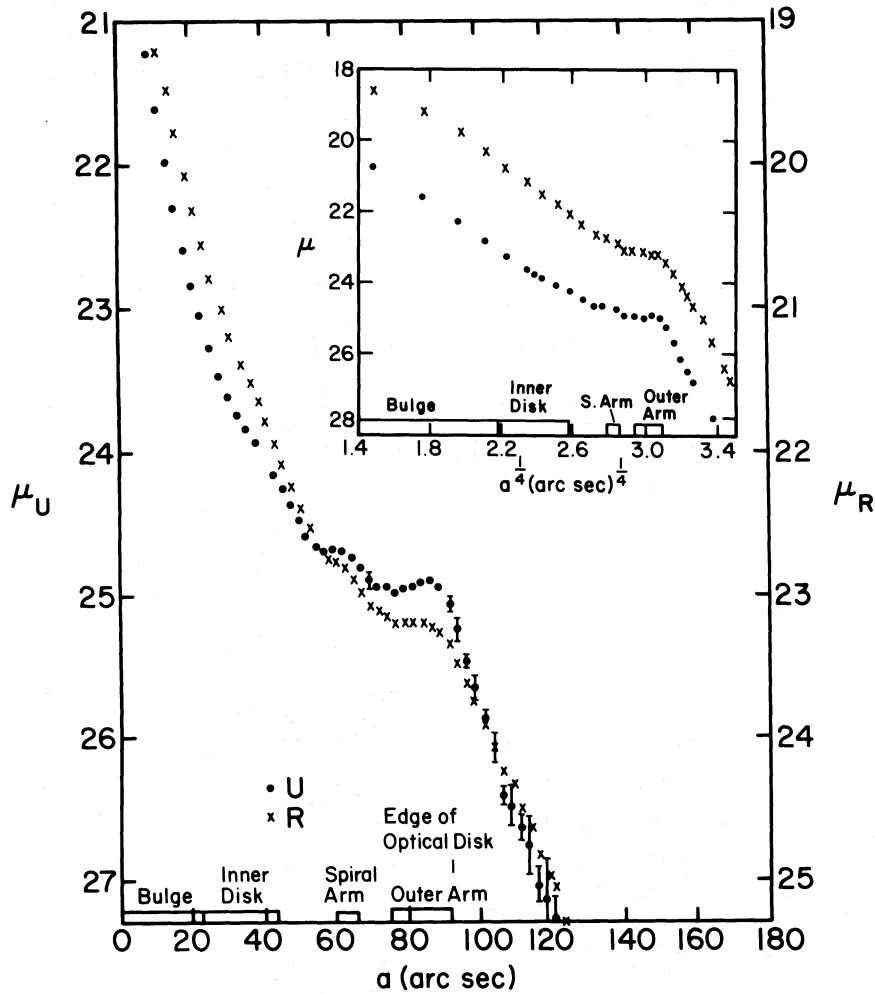


FIG. 4.— U and R surface brightness profiles as a function of nuclear distance; note that the U profile has been normalized to match the R profile at $r = 55''$. The location and blueness of the spiral arms at $r = 62''$ and $r = 87''$ are apparent. (Inset) Surface brightness profiles in U and R as a function of $r^{1/4}$. Interior to $r = 30''$ over the nuclear bulge, the $r^{1/4}$ law is an excellent match to the data.

line intensities in NGC 4378 also shows qualitative similarities to galaxies comparable to our own. The nucleus shows a strong red stellar continuum with emission lines of $[\text{N II}]$ stronger than $\text{H}\alpha$. Measured intensities give $[\text{N II}] \lambda 6548$, $\text{H}\alpha$, and $[\text{N II}] \lambda 6583$ relative values of 2.0, 1.0, and 6.4, respectively, and equivalent widths of 1.5, 1.0, and 5.0 \AA , respectively. Even with a correction of several angstroms for an underlying stellar absorption feature at $\text{H}\alpha$, $[\text{N II}]$ is still more intense than $\text{H}\alpha$ in the nucleus and remains stronger than $\text{H}\alpha$ throughout the bulge ($r \approx 5$ kpc). While it is not unusual to observe $[\text{N II}]$ to be more intense than $\text{H}\alpha$ in galactic nuclei, it is extremely rare (see Jensen, Strom, and Strom 1976) to see this ratio persisting into the disk (although NGC 4594 has been shown by Schweizer 1978 to have a similar intensity ratio at very great galactocentric distances). Only in the H II regions at $r > 10$ kpc do we observe $\text{H}\alpha$ to be more intense than $[\text{N II}]$; $\text{H}\alpha/[\text{N II}] = 3.2$ in

the strongest knot north of the nucleus (Fig. 1), and $\text{H}\alpha/[\text{N II}] > 4$ in the weaker knots. This decrease in the $[\text{N II}]/\text{H}\alpha$ ratio across disks of galaxies is generally interpreted (Searle 1971; Smith 1975) as reflecting an increase in nitrogen abundance toward the nucleus. However, as Searle (1976) has stressed, this explanation probably does not hold in the nucleus where the sizes of H II and N II regions are almost certainly not identical. It would be of considerable interest, although extremely difficult, to measure such ratios as $[\text{O III}]/\text{H}\beta$ and $[\text{N II}]/[\text{O II}]$ for a selection of H II regions in NGC 4378. Such a study would permit a more quantitative discussion of the variation of N and O with radius in this earlier-type system. Moreover, it would then be possible to judge whether the mean chemical abundance in the disk gas of NGC 4378 is consistent with the relatively high values expected for early Hubble types (Smith 1975). Knowledge of the distribution of element abundances in NGC 4378

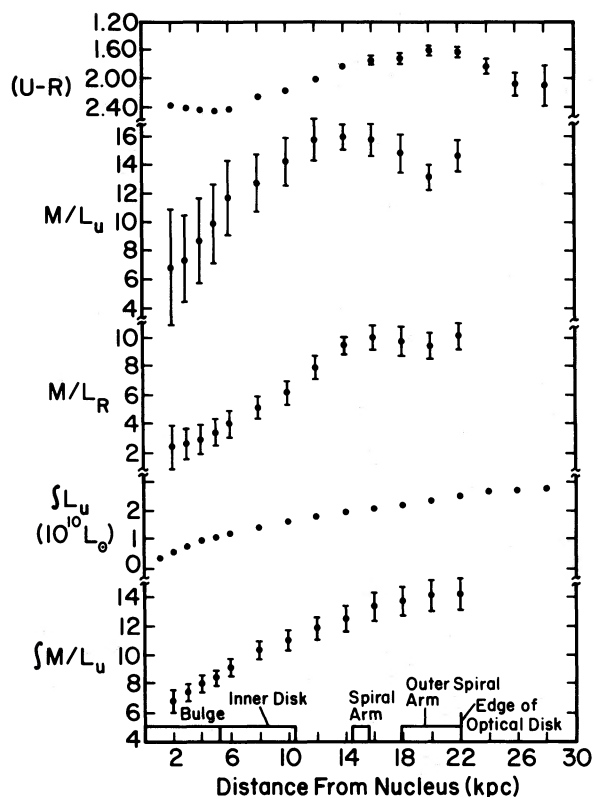


FIG. 5 (top to bottom).—(a) Variation of $(U - R)_0$ as a function of nuclear distance (the increasing blueness of the outer arms is apparent). (b) The local mass to U -luminosity ratio as a function of nuclear distance. (c) The local mass to R -luminosity ratio as a function of nuclear distance. (d) The integrated U luminosity as a function of nuclear distance. (e) The integrated mass to U -luminosity ratio as a function of nuclear distance. For all plots the error bars mark the $\pm 1 \sigma$ range.

clearly would be of value in furthering our understanding of the chemical history of spiral galaxies for a variety of Hubble types.

IV. MASS-TO-LIGHT RATIO WITHIN NGC 4378

We can use the surface brightness and mass distribution determined in the preceding sections to derive the mean mass-to-light ratio \mathfrak{M}/L for NGC 4378. This quantity, as well as its radial variation, is of particular interest in view of the recent proposals suggesting that galaxy halos might be characterized by very large values of \mathfrak{M}/L (e.g., Ostriker, Peebles, and Yahil 1974); as yet, very few values of \mathfrak{M}/L are available for early-type spirals.

In Table 7, columns (2) and (3), we list the surface luminosities per square arcsec in U and R , corrected for extinction and geometrically corrected to face-on (no photometric face-on corrections were made). Using the face-on surface densities for the composite mass model, we calculate the local values of \mathfrak{M}/L as a function of nuclear distance in NGC 4378; these are tabulated in Table 7, columns (4) and (5), and are plotted in Figures 5b and 5c. Locally, the \mathfrak{M}/L_U ratio

increases from about 7 in the bulge to 16 in the disk and then decreases slightly where the U luminosity increases across the outer arm. Values of \mathfrak{M}/L_R locally also increase outward from the nucleus; they rise from 2 to 8 and then remain constant across the outer arms.

The behavior of the integrated \mathfrak{M}/L ratio as a function of r reflects the same general characteristics. The integrated U luminosity, as a function of distance from the nucleus, is tabulated in column (6) of Table 7 and plotted in Figure 5d. (Note that we have not used the R surface brightness to form an integrated R magnitude because the R plate is overexposed for galactocentric distances $r \lesssim 10''$.) The luminosity $L_U = 1 \times 10^{10} L_\odot$ in the region where the nuclear bulge merges with the disk, increases to $L_U = 2.5 \pm 0.08 \times 10^{10} L_\odot$ at the outer edge of the optical image, and continues to increase slowly beyond the apparent optical image until it is lost in the noise of the photographic plate. The absolute magnitude is $M_0(U)_{r=22} = -20.47 \pm 0.02$ or $M_0(U)_{r=28} = -20.57 \pm 0.02$. The integrated mass to U -luminosity ratio, based on the composite mass model, is listed in column (7) of Table 7 and plotted in Figure 5e. The ratio increases with increasing nuclear distance from $\mathfrak{M}/L_U = 6 \pm 1$ at $r = 2$ kpc to $\mathfrak{M}/L_U = 14 \pm 1$ at $r = 22$ kpc. Because the mass to blue-luminosity ratio has been tabulated in the literature for a large sample of galaxies, we would like to convert from U luminosity to B luminosity. For the nucleus of NGC 4378 ($r \leq 3.9$ kpc), $(U - B)_0 = 0.57$ mag; because the disk is bluer than the nucleus, an integrated value of $(U - B)_0 \approx 0.5$ might be a more appropriate estimate. For values in the range $0.5 < (U - B)_0 < 0.57$, the mass to blue-luminosity ratio $\mathfrak{M}/L_B \approx 10$. The derived mean \mathfrak{M}/L for NGC 4378 supports the conclusion that this ratio is low ($\lesssim 20$) for early-type systems, as Faber and Jackson (1976) have stressed. Visvanathan and Griersmith (1977) recently obtained V magnitudes of NGC 4378 through apertures of radii of $23''$, $32''$, and $45''.5$. When these values are corrected for galactic extinction and for inclination and are then combined with our derived mass, we compute integrated values of $\mathfrak{M}/L_V = 3.9$, 5.0, and 5.9 for $r = 5.95$, 8.33, and 11.90 kpc, respectively. To transform our derived values of \mathfrak{M}/L_U to \mathfrak{M}/L_V , we adopt $U - V = 1.6$; then $\mathfrak{M}/L_V = 0.47\mathfrak{M}/L_U$. From Table 7, column (7), we determine $\mathfrak{M}/L_V = 4.3$, 4.9, and 5.6, respectively, at these radii, in excellent agreement with the Visvanathan and Griersmith values.

We note that the outer parts of the galaxy rotational velocities do not exhibit a Keplerian turnover; rather, our mass models suggest that mass increases linearly with r to the limit of our observations. However, the derived values of \mathfrak{M}/L for NGC 4378 lie well below the value of several hundred required to explain the group and cluster "missing mass" (see, for example, Ostriker *et al.*). If a significant mass component of very low luminosity objects extends beyond $r = 22$ kpc, there is virtually no hope of detecting its presence from an optical rotation curve in that region. Thus emphasis should be placed on attempts to detect

neutral hydrogen beyond the optical disk in order to estimate more accurately the true mass and mass distribution for this galaxy.

V. DISCUSSION

In the preceding sections we have determined physical parameters for NGC 4378, an early-type (Sa), apparently anemic spiral. It is of some interest to compare NGC 4378 with other spiral galaxies. An examination of galaxies in the Hubble Atlas (Sandage 1961) reveals that an anemic spiral structure and almost circular arms are the rule rather than the exception for Sa galaxies. This is emphasized by the reclassification of the Hubble Atlas spirals by van den Bergh (1976). Only one galaxy, the Sombrero, retains its Sa classification. All other galaxies are reclassified Aa, i.e., anemic, or of later type.

a) Rotational Properties and the Distance to NGC 4378

On the basis of its central velocity $V_0 = 2427 \text{ km s}^{-1}$ and a Hubble constant $H = 50 \text{ km s}^{-1} \text{ Mpc}^{-1}$, we have adopted a distance of 49 Mpc for NGC 4378. Tully and Fisher (1977) have shown that the width of the 21 cm velocity profile corrected to face-on, $\Delta V/\sin i$ —i.e., twice the maximum rotational velocity—is well correlated with intrinsic galaxy luminosity. On the basis of distances to nearby galaxies, Sandage and Tammann (1976) have shown that the calibration

$$M_{\text{pg}} = -6.88 \log \left(\frac{\Delta V}{\sin i} \right) - 2.36$$

is consistent with $H = 50 \text{ km s}^{-1} \text{ Mpc}^{-1}$. The 21 cm observations of NGC 4378 (Krumm and Salpeter 1976) give $\Delta V = 370 \text{ km s}^{-1}$, from which $M_{\text{pg}} = -21.69$. With $m_U = 12.88$ (Table 8) or $m_B = 12.3$, the 21 cm velocity width calibration gives $r = 63 \text{ Mpc}$, in only fair agreement with the distance determined from the central velocity. Note that the optical velocities (Fig. 2) give $\Delta V = 375 \text{ km s}^{-1}$, in excellent agreement with the 21 cm value. Tully and Fisher (1977) have suggested an alternative calibration,

$$M_{\text{pg}} = -6.26 \log \left(\frac{\Delta V}{\sin i} \right) - 3.5,$$

leading to a higher value for H . With this calibration, the distance to NGC 4378 is $r = 48 \text{ Mpc}$. We do not, however, place any great significance on the somewhat better agreement of our distance determination with the Tully and Fisher value.

b) Neutral Hydrogen Properties of NGC 4378

Krumm and Salpeter (1976) have reported the detection with the Arecibo radio telescope of 21 cm emission from NGC 4378 when the 1.9 beam is centered at the nucleus and at points 1.9 (27 kpc) east and west of the nucleus. The observed flux density out to ± 1.9 is 6.6 Jy km s^{-1} , which corresponds to a hydrogen mass $\mathfrak{M}_{\text{HI}} = 3.7 \times 10^9 \mathfrak{M}_\odot$. With this value

of \mathfrak{M}_{HI} , the hydrogen-mass to U -luminosity ratio $\mathfrak{M}_{\text{HI}}/L_U = 0.15$ (corresponding to $\mathfrak{M}_{\text{HI}}/L_B = 0.1$), while the hydrogen-mass to total-mass ratio $= \mathfrak{M}_{\text{HI}}/\mathfrak{M} = 0.01$. The values quoted here differ from the values given by Krumm and Salpeter (1976) because we have used significantly different values for the distance, the inclination, and the apparent magnitude. Note that, if the H I diameter is twice the optical diameter and the rotation curve remains approximately flat, a mass $\mathfrak{M} \approx 6 \times 10^{11} \mathfrak{M}_\odot$ out to $r = 44 \text{ kpc}$ is implied.

Typical values for $\mathfrak{M}_{\text{HI}}/L_B$ vary along the Hubble sequence from about 0.1 for S0 and Sa galaxies to 0.8 for late-type spirals and irregulars. Thus the hydrogen mass of NGC 4378 (within 1.9) is quite typical for very early-type galaxies. For the 14 E, S0, and Irr II galaxies detected by Gallagher, Faber, and Balick (1975), $\langle \mathfrak{M}_{\text{HI}} \rangle = 2.0 \pm 0.5 \times 10^9 \mathfrak{M}_\odot$.

The density of neutral hydrogen in NGC 4378 can be estimated by assuming that hydrogen constitutes 1% of the total mass of NGC 4378. The neutral hydrogen density can be modeled by assuming it all to be in the disk; hence it constitutes approximately 2% of the disk mass. At 10 kpc, the derived density of the disk component is $0.03 \mathfrak{M}_\odot \text{ pc}^{-3}$ (eq. [1]); so the H I density is $6 \times 10^{-4} \mathfrak{M}_\odot \text{ pc}^{-3}$. In our Galaxy the density of H I is about $7 \times 10^{-3} \mathfrak{M}_\odot \text{ pc}^{-3}$ (Burton 1976), a factor of 10 times that in NGC 4378. Even when one allows for the uncertainties of the model, there seems to be no doubt that the neutral hydrogen density is very low in NGC 4378. Unfortunately, it is quite difficult to ascertain whether our derived hydrogen density is typical of Sa galaxies, since neutral hydrogen observations of galaxies of this type are rare. Roberts's (1969) compilation contains only one Sa and one Sab, while recent observations of early-type galaxies are restricted generally to E, S0, and S0+ classifications.

c) Relation of NGC 4378 to the Two-dimensional Classification of Disk Galaxies by Wakamatsu

Wakamatsu (1976) and Yoshizawa and Wakamatsu (1975) have shown that properties along the Hubble sequence correlate well with the disk-to-bulge ratio which they characterized by three parameters: $K = V_{\text{max}}^2/r_{\text{max}}$, the centrifugal force at the radius r where the rotational velocity is a maximum; $\beta = r_{\text{Hol}}/r_{\text{max}}$, the ratio of the Holmberg radius to r_{max} ; and $\gamma = L_b/L_D$, the ratio of the observed total bulge luminosity to disk luminosity. The relationships between these parameters, which they derive for disk galaxies with known dynamical properties, are reproduced in Figures 6. It should be noted that only two early-type galaxies, NGC 3115 (E7/S0) and M81 (Sab), were used in defining these relationships. For NGC 4378, we compute values of $K = 34 \times 10^3 \text{ km}^2 \text{ s}^{-2} \text{ kpc}^{-1}$, $\beta = 9.5$, and $\gamma \approx 1$. The Holmberg radius is taken to be $120''$ (28 kpc; $M_U \approx 27 \text{ mag arcsec}^{-2}$), and L_b/L_D is assumed to be near unity. (Extrapolation of the bulge luminosity into the disk region and extrapolation from the disk into the bulge give values of γ of slightly greater than and slightly less than unity,

TABLE 8
PARAMETERS FOR NGC 4378 AND NGC 4594, THE SOMBRERO

	NGC 4378	NGC 4594
l,b	286°; +66°9	298°; +51°2
Type	Sa	Sa
van den Bergh (1976)	AbII:	Sa
m _b (de Vaucouleurs <i>et al.</i> 1976)	12.3	9.4
Distance (Mpc)	49	18.2 (Schweizer 1978) 18.6 (Faber <i>et al.</i> 1977)] Adopt 18.4
D ₀ (corrected face-on diam.)	3:2 = 46 kpc	7:4 = 40 kpc
M ₀ (B)	-21.1	-22.35
(U - B) ₀	0.57	0.525 (Table 5)
(B - V) ₀	0.94	0.95
(V - R) ₀	0.77	
σ _v (km s ⁻¹)	190±25	
([NII]/Hα) _{nucl}	5/1	
(Hα/[NII]) _{HII}	>3.2/1	≥3.2/1 (Schweizer 1978)
ΔV ₂₁ /km s ⁻¹	370 (Krumm & Salpeter 1976)	790 (Faber <i>et al.</i> 1977)
ΔV ₂₁ /sin i km s ⁻¹	645	790
V _{max} (km s ⁻¹)	320	≥343 (Schweizer 1978)
r _{max} (kpc)	3	≥14.5 kpc (Schweizer 1978)
K = V _{max} ² /r _{max}	34	~8
β = r _{Holm} /r _{max}	9.5	~4
γ = L _{bulge} /L _{disk}	~1	
M _{tot}	3.6±0.5 10 ¹¹ M _⊙ (r=22 kpc)	3.6±0.6 10 ¹¹ M _⊙ (Faber <i>et al.</i> + Schweizer/2)
M _{HI}	3.7 × 10 ⁹ M _⊙ (r ~ 40 kpc)	9±3 10 ⁸ M _⊙
M _{HI} /L _{opt} (B)	0.10	0.0069±0.0021 (Faber <i>et al.</i> 1977)
M _{HI} /M _{tot}	0.01	0.003
M _{tot} /L _{opt} (B)	10±1	3.7±1 (Schweizer 1978)

respectively.) The location of NGC 4378 on the Wakamatsu plots is indicated by the open circle. For each correlation, NGC 4378 falls at or near the extreme limits for an early-type spiral. We conclude that, while the dynamical properties of NGC 4378 place it at one end of the Hubble sequence, its properties are not abnormal.

d) *A Comparison of NGC 4378 and NGC 4594 (the Sombrero)*

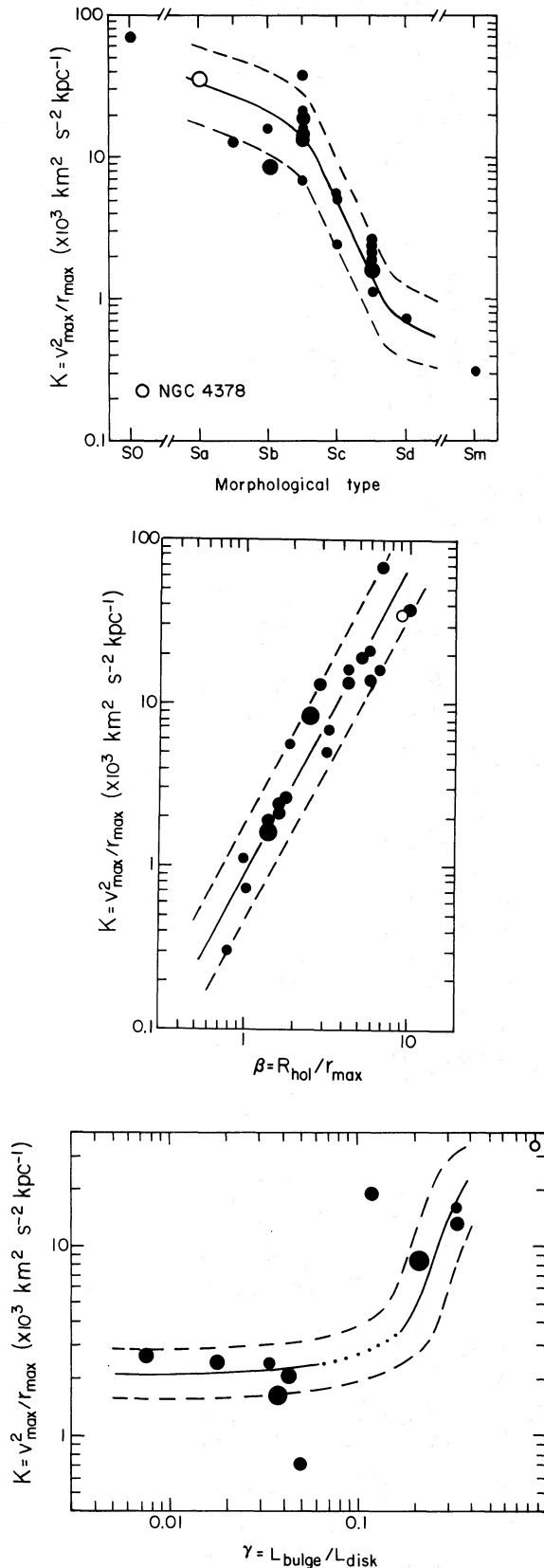
Many properties of NGC 4378 and NGC 4594 are similar. This suggests that NGC 4378, if viewed closer to edge-on, would resemble the Sombrero. We show in Figure 7 (Plate 8) a 4 m plate of NGC 4594 kindly made available by Dr. F. Schweizer, and compile in Table 8 physical and dynamical parameters for the two galaxies.

Both galaxies have old nuclear populations, enriched gas extending well into the disk, normal outer H II regions, high rotational velocities, large total masses, and low hydrogen masses. For NGC 4378 the maximum rotational velocity comes within a few kiloparsecs of the nucleus; for NGC 4594 it has not been reached at 14.5 kpc, almost the edge of the optical

image. A major difference between the two galaxies is in the neutral hydrogen content, which is low for both galaxies but almost a factor of 5 lower in NGC 4594 than in NGC 4378. Although we have comparable parameters for no other Sa galaxies, we see no evidence that this range is abnormal, and suggest that NGC 4378 and NGC 4594 reveal the range of parameters within the Hubble class Sa.

e) *The Anemic Appearance of NGC 4378*

The *U* and *R* surface brightness distributions derived for NGC 4378 provide the basis for a more quantitative discussion of its anemic appearance. From the data listed in Table 6 and plotted in Figure 4, we can first compare the parameters describing the disk of NGC 4378 with those derived for other disk galaxies. We determined (according to the procedure outlined by Freeman 1970) the best-fit exponential [$\mu \approx \mu(0) \exp(-\gamma r)$] to the *U* and *R* surface brightness profiles for two regions of the disk. Region 1 covers the range of galactocentric distances $20'' \lesssim r \lesssim 40''$, while region 2 covers the range $r > 50''$, but excluding the strong arms. For region 1, we derive a projected central surface brightness $\mu_B(0) \approx 21.6$ mag



arcsec $^{-2}$, $\gamma^{-1} = 23''$ (5.5 kpc), while for region 2, $\mu_B(0) \approx 22.3 \text{ mag arcsec}^{-2}$, $\gamma^{-1} = 28''$ (6.7 kpc). We assumed an average $U - B$ and $B - R$ of 0.5 and 1.7, respectively, in order to transform U and R surface brightnesses to equivalent B -values. The first value of $\mu_B(0)$ is almost identical to the "universal" value of $21.65 \text{ mag arcsec}^{-2}$ derived by Freeman from analysis of 36 disk systems. The second value, while nearly a factor of 2 smaller, lies within 2 standard deviations of the universal value of $\mu_B(0)$. Hence the projected central surface brightness deduced from the disk light distribution in NGC 4378 might be termed "marginally lower" than in other disk systems. The exponential scale lengths derived for the disk lie in the mid-range of Freeman's derived values for early-type spirals.

Kormendy (1977) has criticized the Freeman fitting procedure, because in many systems the nuclear bulge contributed a nonnegligible fraction of the total light, even in regions apparently dominated by the disk. He therefore fits the nuclear-bulge-dominated region to a de Vaucouleurs profile and subtracts the best-fit bulge profile from the galaxy light distribution; the remainder is attributed to the disk contribution. For a limited sample of S0 galaxies, Kormendy finds that the brightest parts of the disk range in surface brightness from $\mu_B \approx 22.5 \text{ mag arcsec}^{-2}$ to $\mu_B \approx 25 \text{ mag arcsec}^{-2}$. For NGC 4378, we find that the brightest part of the disk has a surface brightness $\mu_B \approx 24.5 \text{ mag arcsec}^{-2}$. Hence the disk surface brightness for this galaxy, while within the limits found by Kormendy, has a somewhat lower maximum surface brightness than most disks. Therefore, we conclude that the anemic appearance of NGC 4378 may arise, in part, from a disk surface brightness somewhat lower than that characteristic of normal galaxies. A firmer statement would be possible were more accurate surface brightness profiles available for a wider range of S0 and spiral galaxies.

From examination of Figure 4, we can estimate the maximum arm amplitude for NGC 4378: In R the arm light exceeds the disk light by a factor of 1.4. This value is quite typical of the maximum arm amplitude found by Schweizer (1976) from analysis of the R light distributions in his sample of six spiral galaxies. However, the difference in $U - R$ color between the arm and disk regions is considerably smaller in NGC 4378 (0.3 mag) than in the typical spiral in Schweizer's sample (0.9 mag). Because the arm colors in NGC 4378 are redder by nearly 0.6 mag than those characteristic of other spirals, we speculate that the star-formation efficiency in this galaxy is lower than "normal." Hence the apparent anemia of NGC 4378 may result not only from the relative faintness of the disk but also from a lower rate of star formation.

The apparently low star-forming efficiency in the

FIG. 6.—Location of NGC 4378 on the two-parameter plots of Wakamatsu (1976). In all representations, NGC 4378 is located at one end of the distributions. We thank Dr. Wakamatsu and the editors of the *Publications of the Astronomical Society of Japan* for granting permission to reproduce his published plots.

arms of NGC 4378 may be caused, in part, by the lower than normal hydrogen density estimated for this galaxy. Another contributing factor is suggested by the work of Roberts, Roberts, and Shu (1975). These authors argue that star formation is triggered by post-shock compression of disk gas as it flows through the density-wave pattern in the disk stars. If the velocity of the gas which is normal to the arm pattern, w_{\perp} , exceeds the sound speed of the gas by a large factor, the gas compression and the presumed star-formation efficiency are both high (see also Jensen *et al.*). If w_{\perp} is small, the compression and star-forming efficiency are low. The value of w_{\perp} can be computed from

$$w_{\perp} = [\Omega(r) - \Omega_p]r \sin i.$$

Here $\Omega(r)$ is the angular velocity of the gas (or stellar) component at r , while Ω_p is the angular speed of the arm pattern. The quantity i is the pitch angle of the arms; for tightly wound spirals, i is small, while for open patterns, i is large. For NGC 4378, we estimate Ω_p as $13 \text{ km s}^{-1} \text{ kpc}^{-1}$ from the observed velocity of the outermost H II region at $r = 22 \text{ kpc}$ (Roberts *et al.*). Near the prominent spiral arms between 14 and 18 kpc, $\Omega(r) \approx 18 \text{ km s}^{-1} \text{ kpc}^{-1}$. Hence, in the arm regions, $w_{\perp} = 80 \sin i \text{ km s}^{-1}$. From examination of the spiral pattern in NGC 4378, we estimate that $i \lesssim 5^\circ$, so that $w_{\perp} \lesssim 7 \text{ km s}^{-1}$. For disk gas with an electron temperature near 10^4 K , the sound speed is $\sim 8 \text{ km s}^{-1}$. Therefore, the compression and presumably the star-forming efficiency in the arm regions of NGC 4378 are expected to be small.

VI. CONCLUSIONS

From a combined spectroscopic and photometric study of NGC 4378, we draw the following conclusions:

1. NGC 4378 is located at a distance of 49 Mpc and is not a member of the Virgo cluster. This distance is consistent both with its velocity $V_0 = 2427 \pm 10 \text{ km s}^{-1}$ ($H = 50 \text{ km s}^{-1} \text{ Mpc}^{-1}$) and the luminosity determined from its H I and optical velocity profile. At this distance, the absolute U magnitude $M_0(U) = -20.7$.

2. Rotational velocities in NGC 4378 rise steeply to $V_{\text{max}} = 320 \text{ km s}^{-1}$ at $r \leq 3 \text{ kpc}$, then decrease only as $V \propto r^{-0.05}$ to $V = 286 \text{ km s}^{-1}$ at $r = 22 \text{ kpc}$, the edge of the optical disk. Only NGC 4594, the Sombrero, has a higher known V_{max} .

3. A composite mass model consisting of a spheroidal bulge ($c/a = 0.8$) and a flattened spheroidal disk ($c/a = 0.2$), both with densities decreasing according to a simple model, will reproduce the observed velocities. The mass rises linearly with r to the outer edge of the optical image; $\mathfrak{M} = 3.6 \pm 0.5 \times 10^{11} \mathfrak{M}_{\odot}$ within $r = 22 \text{ kpc}$. The bulge component contains 60% of the total mass.

4. The surface brightness profiles in U and R both decrease as $r^{1/4}$ within the nuclear bulge, but thereafter decrease only slowly across the disk and arms. The disk surface brightness profile does not appear to have the well-defined exponential character of many spiral galaxies.

5. The integrated mass to U -luminosity ratio increases from $\mathfrak{M}/L_U = 6 \pm 1$ at small r to $\mathfrak{M}/L_U = 14 \pm 1$ for the entire galaxy. From this, $\mathfrak{M}/L_B \approx 10$.

6. The hydrogen mass within $r \approx \pm 40 \text{ kpc}$ is $\mathfrak{M}_{\text{HI}} = 3.7 \times 10^9 \mathfrak{M}_{\odot}$ (Krumm and Salpeter 1976), $\mathfrak{M}_{\text{HI}}/L_B = 0.1$, and $\mathfrak{M}_{\text{HI}}/\mathfrak{M}_{\text{total}} = 0.01$. These values are consistent with the range of values characterizing the rather limited sample of early-type systems surveyed to date.

7. The disk of NGC 4378 contains ionized hydrogen knots. Measurement of emission-line strengths in these knots reveals [N II] stronger than H α in the inner disk but weaker than H α in the outermost H II regions. This behavior is consistent with that observed in other early-type spiral galaxies in which the nitrogen-to-hydrogen ratio is inferred to decrease with increasing galactocentric distance.

8. The $U - R$ color index is constant over the nuclear bulge, then becomes blue in those regions of the disk characterized by active star formation, as evidenced by the presence of H II complexes in the arm region. Beyond the outermost arm, the disk color again reddens. Within the bulge, the relative U luminosity to R luminosity $L_U/L_R = 0.35 \pm 0.01$, while at the edge of the optical image it has increased to $L_U/L_R = 0.70 \pm 0.05$.

9. NGC 4378, if viewed edge-on, would resemble the Sombrero galaxy. The Hubble classification, V_{max} , emission-line strength, mass, color, and \mathfrak{M}/L ratio are similar, although the hydrogen mass is 5 times higher in NGC 4378. In spite of its extremely weak spiral structure, NGC 4378 appears to have a normal stellar population with galactic parameters which place it at the high bulge-to-disk ratio, high mass, and high rotational-velocity end of the Hubble spiral sequence.

10. The anemic appearance of the galaxy results, in part, from a somewhat lower than normal disk surface brightness and from an apparently lower rate of star formation than is typical of well-studied spiral galaxies. The low star-formation rate may, in turn, result from a combination of low disk-hydrogen density and the unfavorable conditions in NGC 4378 for high gas compression in spiral shocks.

We thank Dr. Victor Blanco, Director of CTIO, for telescope time and E. Cosgrove for his capable assistance at the telescope. We acknowledge valuable conversations with Drs. W. Herbst, C. Krishna Kumar, J. Lockman, C. J. Peterson, R. Sinha, F. Schweizer, and N. Thonnard.

REFERENCES

- Brandt, J. C. 1960, *Ap. J.*, **131**, 293.
 Burbidge, E. M., Burbidge, G. R., and Prendergast, K. H. 1959, *Ap. J.*, **130**, 739.
 Burton, W. B. 1976, *Ann. Rev. Astr. Ap.*, **14**, 275.
 de Vaucouleurs, G. 1959, *Handbuch der Physik*, **53**, 311.
 ———. 1961, *Ap. J. Suppl.*, **5**, 233.

- de Vaucouleurs, G., de Vaucouleurs, A., and Corwin, H. G. 1976, *Second Reference Catalogue of Bright Galaxies* (Austin: University of Texas Press).
- Faber, S. M., Balick, B., Gallagher, J. S., and Knapp, G. R. 1977, *Ap. J.*, **214**, 383.
- Faber, S. M., and Jackson, R. E. 1976, *Ap. J.*, **204**, 668.
- Freeman, K. C. 1970, *Ap. J.*, **160**, 811.
- Gallagher, J. S., Faber, S. M., and Balick, B. 1975, *Ap. J.*, **202**, 7.
- Jensen, E. B., Strom, K. M., and Strom, S. E. 1976, *Ap. J.*, **209**, 748.
- Kormendy, J. 1977, *Ap. J.*, **214**, 359.
- Krumm, N., and Salpeter, E. E. 1976, *Ap. J. (Letters)*, **208**, L7.
- Kuzmin, G. G. 1952, *Pub. Astr. Obs. Univ. Tartu*, **32**, 211.
- Nilson, P. 1973, *Uppsala General Catalogue of Galaxies (Uppsala Obs. Ann., Vol. 6)*.
- Ostriker, J. P., and Peebles, P. J. E. 1973, *Ap. J.*, **186**, 467.
- Ostriker, J. P., Peebles, P. J. E., and Yahil, A. 1974, *Ap. J. (Letters)*, **193**, L1.
- Peterson, C. J., Rubin, V. C., Ford, W. K., and Thonnard, N. 1976, *Ap. J.*, **208**, 662.
- Roberts, M. S. 1969, *A.J.*, **74**, 859.
- Roberts, W. W., Roberts, M. S., and Shu, F. H. 1975, *Ap. J.*, **196**, 381.
- Sandage, A. 1961, *The Hubble Atlas of Galaxies* (Washington: Carnegie Institution of Washington).
- . 1977, unpublished.
- Sandage, A., Becklin, E. E., and Neugebauer, G. 1969, *Ap. J.*, **157**, 55.
- Sandage, A., and Tammann, G. A. 1976, *Ap. J.*, **210**, 7.
- Schweizer, F. 1976, *Ap. J. Suppl.*, **31**, 313.
- . 1978, *Ap. J.*, **220**, 98.
- Searle, L. 1971, *Ap. J.*, **168**, 327.
- . 1976, in *The Galaxy and the Local Group*, ed. R. J. Dickens and J. E. Perry (*RGO Bull.*, No. 182, p. 119).
- Smith, H. E. 1975, *Ap. J.*, **199**, 591.
- Strom, K. M., and Strom, S. E. 1977, in *The Evolution of Galaxies and Stellar Populations*, ed. B. M. Tinsley and R. B. Larson (New Haven: Yale University Observatory).
- Strom, K. M., Strom, S. E., Jensen, E. B., Moller, J., Thompson, L. A., and Thuan, T. X. 1977, *Ap. J.*, **212**, 335.
- Tully, R. B., and Fisher, J. R. 1977, *Astr. Ap.*, **54**, 661.
- van den Bergh, S. 1968, *J.R.A.S. Canada*, **62**, 219.
- . 1976, *Ap. J.*, **206**, 883.
- Visvanathan, N., and Griersmith, D. 1977, *Astr. Ap.*, **59**, 319.
- Wakamatsu, K. 1976, *Pub. Astr. Soc. Japan*, **28**, 397.
- Yoshizawa, M., and Wakamatsu, K. 1975, *Astr. Ap.*, **44**, 363.

W. KENT FORD, JR., and VERA C. RUBIN: Department of Terrestrial Magnetism, Carnegie Institution of Washington, 5241 Broad Branch Road, N.W., Washington, DC 20015

W. ROMANISHIN, K. M. STROM, and S. E. STROM: Kitt Peak National Observatory, P.O. Box 26732, Tucson, AZ 85726

PLATE 7

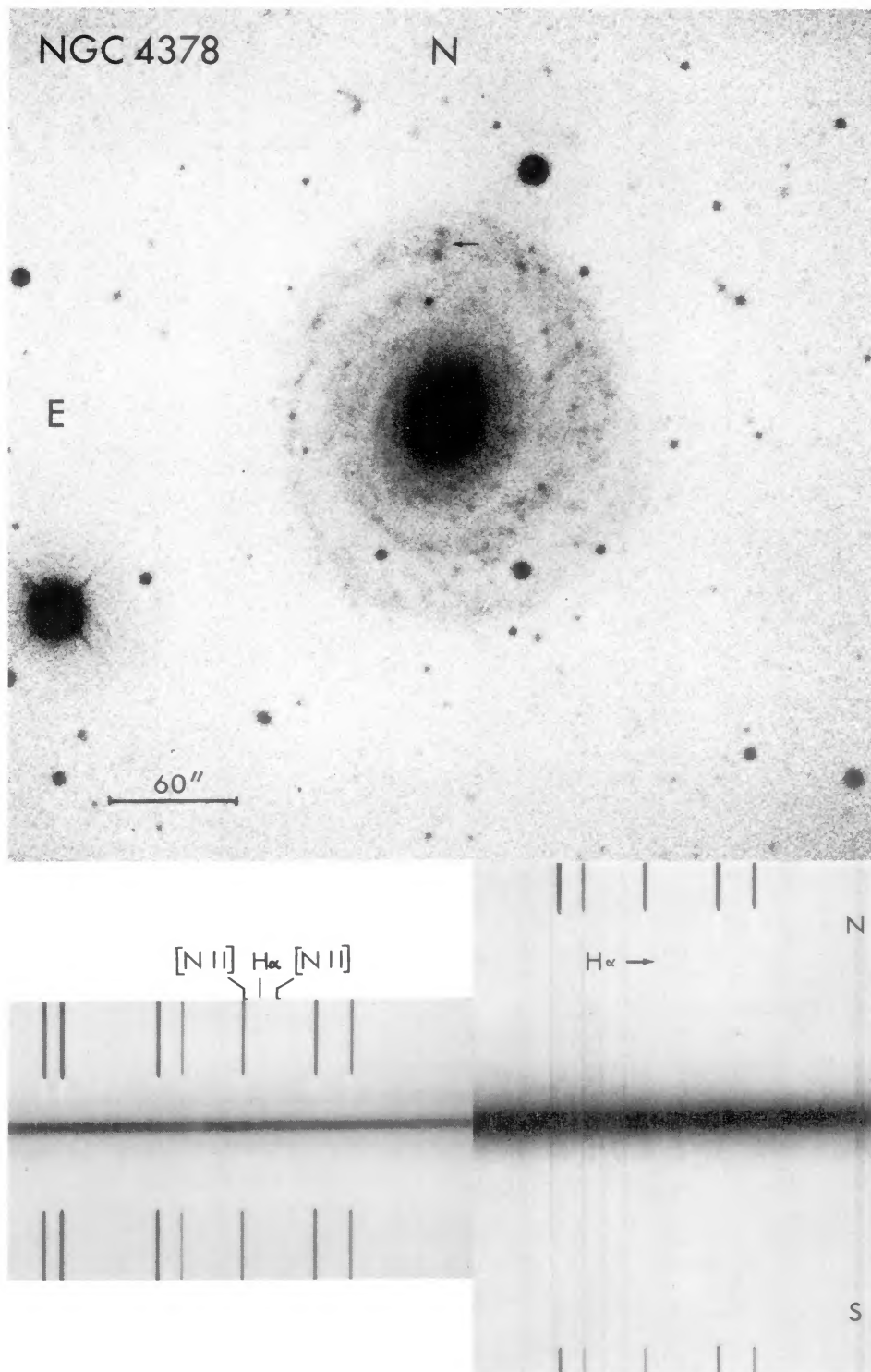


FIG. 1.—(Top) Reproduction of a Mayall 4 m plate of NGC 4378: N₂ baked, hydrogen treated IIIa-J plus UG-2 (ultraviolet) filter, exposure 100 minutes. Arrow in outer arm north of nucleus identifies H II knots whose spectra are shown in bottom right. (Bottom left) Spectrum of nucleus of NGC 4378: plate C460a, N₂ baked plus preflashed IIIa-J, original dispersion 50 Å mm⁻¹, exposure 20 minutes. Note that [N II] is more intense than H α in the nucleus. (Bottom right) Plate C466, P.A. 180°, exposure 150 minutes. Weak H α is visible in outer knots.

RUBIN *et al.* (see page 782)

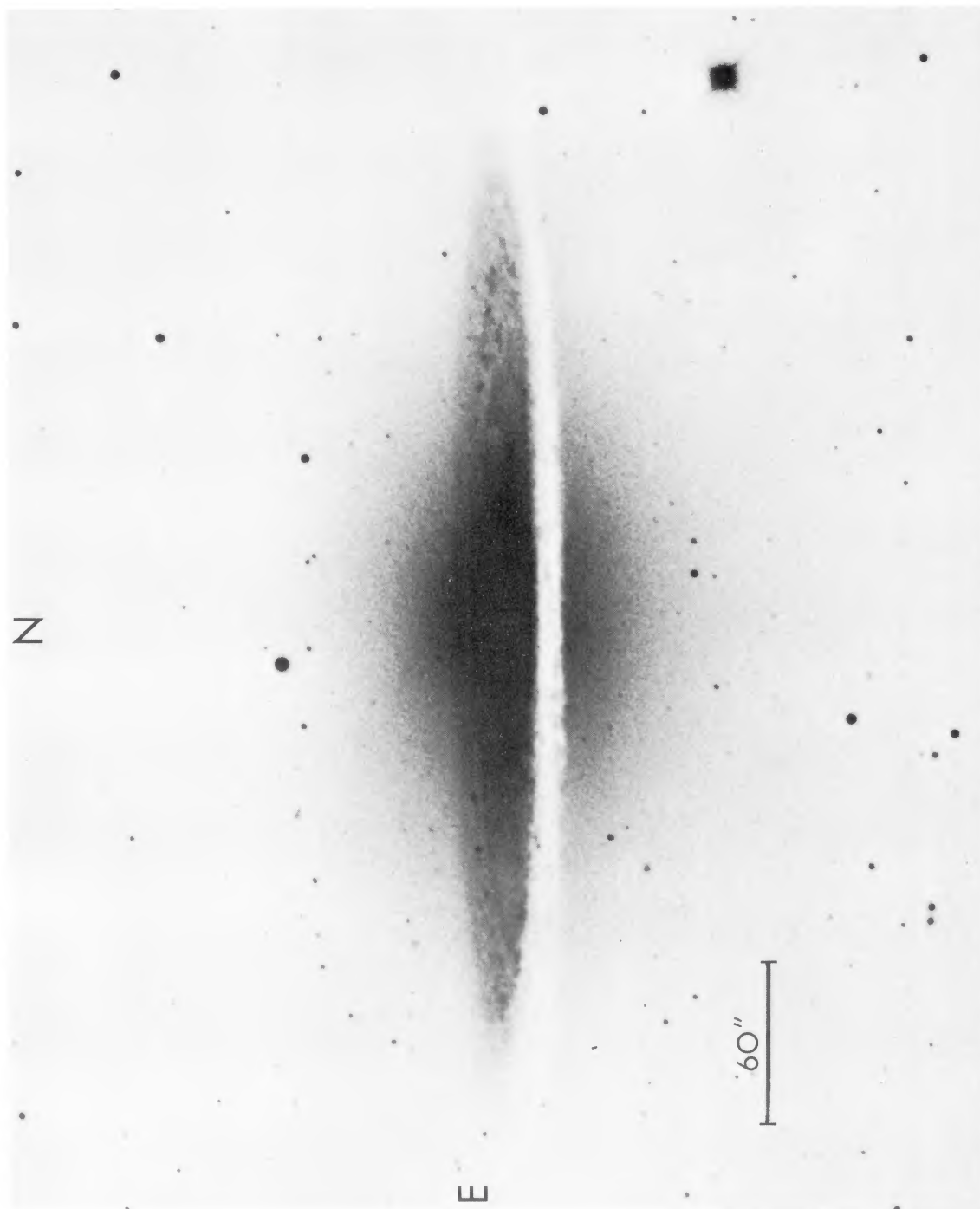


FIG. 7.—NGC 4594 from a CTIO 4 m plate kindly made available by Dr. F. Schweizer. NGC 4378, if viewed more nearly edge-on, should resemble NGC 4594.

RUBIN *et al.* (see page 792)